Tellus (1988), *40A*, 26–36

10-day predictability of the northern hemisphere winter 500-mb height by the ECMWF operational model

By M. DÉQUÉ, *Centre National de Recherches Météorologiques (DMN/EERM), 42 Av. Coriolis, 31057 Toulouse, France*

(Manuscript received November 18, 1986; in final form March 9, 1987)

ABSTRACT

A statistical method is performed on the 10-day forecasts by the European Centre for Medium Range Weather Forecasts (ECMWF) operational model for the 1979/80 to 1985/86 winter 500 mb geopotential heights in order to look for the spatial structures of the field that are best predicted by the model and to evaluate the quality of these optimum predictions by comparing with persistence predictions. It is shown that one index associated with a structure connecting the Pacific negatively to the Atlantic has better skill than the smoothed persistence of any linear combination of the initial state. The same investigations are then carried out on 3 sub-regions of the northern hemisphere: Atlantic-Europe, Asia, and Pacific–North America. The Pacific–North America area has some predictability at 10-day lag, the Atlantic–Europe area a marginal one, and the Asian area no predictability at all (referring to persistence as well as to a randon predictor).

1. Introduction

The predictability limit of Numerical Weather Prediction models is strongly dependent on the kind of prediction we need. For a deterministic prediction of the geographical distribution of a field at a given date, the limit is presently not further than 5 days. For a prediction averaged in space and time, some recent studies (Miyakoda et al., 1986; Cubasch and Wiin-Nielsen, 1986) show that some predictability remains up to 30 days. The difference between these two lags is due to the growth of the error in numerical models that masks the information in the outputs. Since the error is little correlated with time, a way of reducing it is to consider the average over several consecutive days of the forecasts; since it is most important in the small spatial scales, one can also average the forecasts in space. Both ways of reducing the relative part of the error can be improved by averaging over several independent forecasts (Hoffman and Kalnay, 1983). The first way is useful to localize a strong and persistent event, whereas the second one is useful when we need a forecast at a precise date of a large scale phenomenon (e.g., to predict the beginning or the end of a blocking situation). Of course both ways can be used simultaneously for theoretical studies: Cubasch and Wiin-Nielsen (1986) consider 10-day means averaged for spectral wave numbers 1–3. In the following, we shall consider only spatial means. They can be accomplished by a truncation keeping the first spherical harmonics or the first Empirical Orthogonal Functions (EOF) (Peagle and Haslam, 1982). The choice of the first spherical harmonics or EOFs is reasonable, since they correspond to large-scale fluctuations of the atmosphere and are thus less affected by the model noise, but it is not optimal since there is no reason why a spherical harmonic or an EOF or order n should be better predicted than order $n+1$.

The aim of this study is to maximize statistically the predictability in order to investigate the large-scale patterns which are the most predictable. In Section 2, we present the statistical method (2.1) and the data available (2.2). This is followed by an application to the northern hemisphere data (Section 3) and the regional data (Section 4).

2. Predictable component analysis

2.1. The method

Let us consider a field $X(x, t)$, x being the spatial coordinate and t the time. This field, assumed to have a zero time mean, can be expanded as:

$$X(x, t) = a_1(t) A_1 + \ldots + a_n(t) A_n(x) + R_n(x, t) \quad (1)$$

where the $a_i(t)$ are orthonormalized time series:

$$(1/T) \sum_{t=1}^{T} a_i(t) a_j(t) = 1 \quad \text{if } i = j,$$
$$= 0 \text{ otherwise} \quad (2)$$

and $R_n(x, t)$ a remaining term which is 0 when n is large enough or disregarded when truncation is performed. Among the multiple expansions of X the best known is the EOF decomposition (Lorenz, 1956; Holmström, 1963): in this case the property of the expansion is the minimum mean square of R_n, which is equivalent to the maximum mean square of the A_i's. The space mean square of A_i divided by the space time mean square of X is called the part of variance explained by the ith EOF. The EOFs are arranged in decreasing part of variance. The first EOFs express the large scale fluctuations of the field X. The first EOFs of 500 mb height simulated by a model such as the ECMWF atmospheric model are nearly the same as those of the observed data (Volmer et al., 1984; Déqué, 1986a). But this property will not ensure that the corresponding components $a_i(t)$ will be better predicted by the model than any spatial linear combination of the field X. If we consider the predicted field $X^P(x, t)$ provided by the integration of the numerical model and the corresponding components $a_i^P(t)$, obtained by the projection of X^P on the A_i's, maximizing the predictability is equivalent to minimizing the Root Mean Square (RMS) error:

$$e_i = \left[(1/T) \sum_{t=1}^{T} (a_i(t) - a_i^P(t))^2 \right]^{1/2} \quad (3)$$

The solution to this minimization is given by the Predictable Component Analysis (Déqué, 1986b). The diagonalization of a symmetrical matrix leads to a new set of vectors B_i called the predictable axes and corresponding components b_i and b_i^P (for more details see Appendix):

$$X(x, t) = b_1(t) B_1(x) + \ldots + b_n(t) B_n(x) + R_n(x, t), \quad (4a)$$

$$X^P(x, t) = b_1^P(t) B_1(x) + \ldots + b_n^P(t) B_n(x) + R_n^P(x, t). \quad (4b)$$

The b_i's are still orthonormalized and the predictable axes are arranged in increasing RMS error e_i. This error e_i has to be compared with the error e_i' obtained by a trivial way of prediction of the component $b_i(t)$. We have only to consider in (4) the terms corresponding to e_i' greater than e_i since the prediction of the other terms by the model is not of interest. A trivial way of prediction is the autoregressive prediction of order 1 also called smoothed persistence. If we consider forecasts at lag 1, the prediction of $b_i(t)$ would be $AC_i(1)\, b_i(t-1)$ where $AC_i(1)$ is the time autocorrelation of b_i at lag 1. The RMS error of such a prediction is $e_i' = (1 - AC_i(1)^2)^{1/2}$ which is better than pure persistence ($b_i^P = b_i(t-1)$, $e_i' = (2(1 - AC_i(1)))^{1/2}$) or climatology ($b_i^P = 0$, $e_i' = 1$). The predictable part of X by the model is thus the sum of the $b_i(t) B_i(x)$ for i satisfying the condition:

$$e_i < (1 - AC_i(1)^2)^{1/2} \quad (5)$$

The part of variance p_i explained by the ith predictable axis is the mean square of B_i over the mean square of X. It lies between the part of variance explained by the nth EOF and that of the first EOF.

The predictable part of X by the model may be compared with the predictable part by the smoothed persistence. In this case we obtain a new set of vectors C_i called the persistent axes and the corresponding components c_i:

$$X(x, t) = c_1(t) C_1(x) + \ldots + c_n(t) C_n(x) + R_n(x, t), \quad (6)$$

The persistent axes are arranged in decreasing squared autocorrelation at lag 1 of the components, which corresponds to increasing RMS error.

2.2. The data

The analysis described in the last subsection has been carried out on a set of 10-day winter forecasts (l = 10) by the operational ECMWF model from December 1979 to February 1986. This yields 630 forecasts and the corresponding analyses. The field retained for this study is the

500 mb geopotential height since it is currently used in studies of forecast skill (Cubasch and Wiin-Nielsen, 1986). The mean analysed (forecast) 10-day averages from 1 December–10 December to 19 February–28 February have been removed from the daily analyses (forecasts) so that there is neither a seasonal cycle nor a model bias in the data. The fields are truncated in spherical harmonics up to wave number 21 and only the northern hemisphere is considered. The first problem that arises with such data is the non-homogeneity of the forecasts: on 21 July 1982 analysed Sea Surface Temperatures were taken into account, on 21 April 1983 the model was converted to a spectral one (truncation T63), on 1 February 1984 the orography was modified, and on 1 May 1985 the truncation was changed to T106. As we shall see in the next Section (3.4) this did not much alter the statistics of the 10-day forecasts, or at least the alteration was small when compared with the interannual variability of the atmosphere.

The second problem is the shortness of the sample. The 630 situations are not independent. If we roughly apply the analysis, we get a first predictable axis with an RMS error of 0.45 (which is very good: the corresponding correlation anomaly is 0.9) but the part of explained variance is 0.0003%. This axis is purely artificial and depends strongly on the sample. Thus, we have to reduce the number of degrees of freedom, and the best way to do it with a minimum loss of information is to truncate the field by its first n EOFs. The smaller n will provide:

(i) a better statistical stability (n degrees of freedom);
(ii) a higher part of variance (greater than that of the nth EOF);
(iii) a faster computation (diagonalization of a $n \times n$ matrix);
(iv) a higher RMS error.

The first three points are positive but the last one is negative; we thus have to choose a value for n not too large but not too small. For that we shall consider an over-estimate e_i^* of the RMS error; e_i is namely an under-estimate of the RMS error since it is a result of the minimization on a particular sample, and if we should compute the error for winters before 1979 or after 1985, we should probably get a value greater than e_i. Let us therefore consider the following testing procedure for calculating e_i^*:

step 1. We calculate B_i using the sample 1980/81, ..., 1985/86 and project the fields $X(x, t)$ and $X^{\mathrm{P}}(x, t)$ on B_i for $t = 1$, 90 (i.e. winter 1979/80) in order to obtain $b_i^*(t)$ and $b_i^{\mathrm{P}*}(t)$.

step 2. We calculate B_i using the sample 1979/80, 1981/82, ..., 1985/86 and obtain in the same way, $b_i^*(t)$ and $b_i^{\mathrm{P}*}(t)$ for $t = 91$, 180 (winter 1980/81).

⋮

step 7. We calculate B_i using the sample 1979/80, ..., 1984/85 and obtain in the same way, $b_i^*(t)$ and $b_i^{\mathrm{P}*}(t)$ for $t = 541$, 630 (winter 1985/86). Then:

$$e_i^* = \left[(1/630) \sum_{t=1}^{630} (b_i^*(t) - b_i^{\mathrm{P}*}(t))^2 \right]^{1/2} \tag{7}$$

If we now increase the number n of EOF of the truncation we shall first observe a decrease of e_i^* because the field X is better taken into account, but when the details retained by the truncation induce a too large dependence of B_i on the learning sample e_i^* will increase. Table 1 shows

Table 1. *Effect of the truncation by the first n EOFs on the first predictable axis: cumulative part of variance explained by the first n EOFs (v_n), part of variance explained by the first predictable axis (p_1), RMS error with the whole sample (e_1), and with the testing procedure e_1^*)*

n	1	5	10	15	20	25	30	35	40	45	50
v_n	0.112	0.400	0.592	0.704	0.779	0.827	0.862	0.889	0.909	0.925	0.939
p_1	0.112	0.090	0.081	0.078	0.076	0.074	0.073	0.070	0.068	0.068	0.068
e_1	1.031	0.921	0.804	0.782	0.756	0.720	0.731	0.711	0.696	0.685	0.674
e_1^*	1.031	0.940	0.833	0.791	0.802	0.788	0.809	0.798	0.768	0.844	0.810

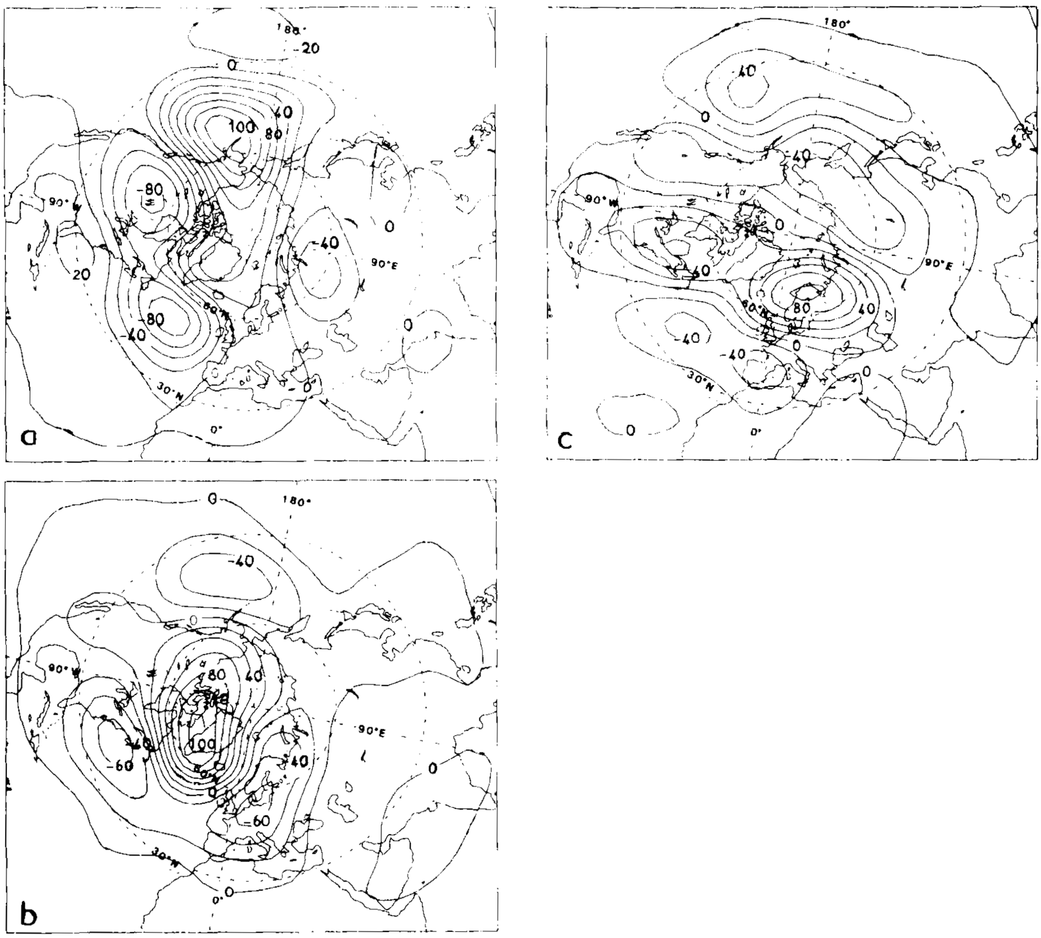

Fig. 1. First (a), second (b), and third (c) EOF of winter 500 mb height (contour interval 20 m).

that the minimum value for e_i^* is reached for $n = 40$ but, since there is a large fluctuation for $n = 45$, we prefer to stay in a range where e_i^* is stable and choose $n = 20$. The truncation keeps 78% of the variance of the field. The difference between $e_1 = 0.76$ and $e_1^* = 0.80$ is small and shows the statistical stability of the method. It may be added that the maps of the first 4 predictable axes are very little dependent on n in the range [10, 50].

3. Predictable part of hemispheric 500 mb height at 10-day lag

3.1. The first EOFs

Before maximizing the predictability let us look at the predictive skill of the first EOFs. The first one (Fig. 1a) explains 11% of the total variance. It represents a contrast between the North Pacific on the one hand and North Atlantic and central Canada on the other. This EOF is not very persistent since its autocorrelation at 10-day lag is 0.02, neither predictable by the model since the RMS error at this lag is 1.03. The second EOF (Fig. 1b) explains 10% of the total variance and exhibits a contrast between polar regions and midlatitudes. It is slightly persistent since the RMS error by smoothed persistence is 0.95 but not predictable by the model since the RMS error is 0.98. The third EOF (Fig. 1c) explains 8% of the variance. The pattern is centred on Scandinavia, negatively correlated with midlatitude Atlantic and eastern Siberia, and positively teleconnected with Labrador and

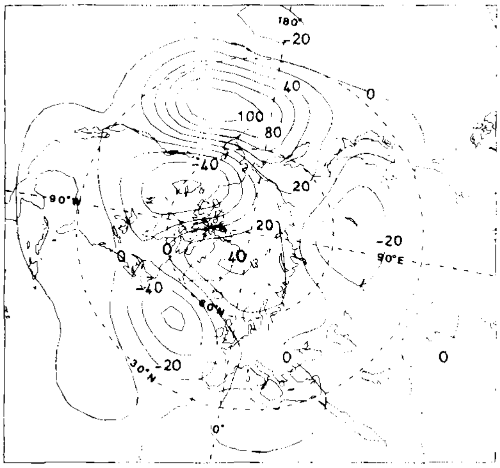

Fig. 2. First predictable axis by the ECMWF model (contour interval 20 m).

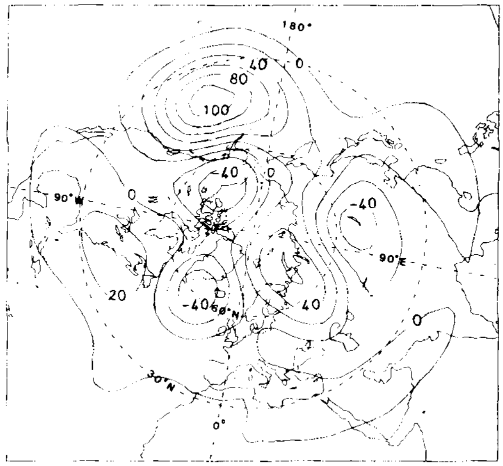

Fig. 3. First persistent axis at 10-day lag (contour interval 20 m).

the midlatitude Pacific. This EOF is not very persistent (the RMS error by smoothed persistence is 0.998) but the model can predict it with a little skill at 10-day lag since the RMS error is 0.92. The following EOFs are neither persistent nor predictable by the model.

3.2. *The first predictable axes*

We have performed the statistical analysis described in Section 2.1 on the 10-day forecasts, filtered by the first 20 EOFs of the 500 mb height field. The first predictable axis (Fig. 2) explains 8% of the total variance: its importance is about the same as the third EOF. The RMS error computed by (3) is $e_1 = 0.76$ and computed by (7) is $e_1^* = 0.80$. This is a good performance since it corresponds to a time anomaly correlation coefficient of 0.7 (it is of the same order as the 4-day lagged autocorrelation of the first EOF). The skill is not only explained by the persistence of the pattern since the RMS error by smoothed persistence is 0.90. The spatial pattern exhibits a strong resemblance with the first EOF. The slight differences are sufficient to increase significantly the predictive skill. The second and third predictable axes have some predictive skill (i.e., the RMS error by the model is less than the error by smoothed persistence) but the RMS error calculated by the testing procedure e_2^* and e_3^* are greater than 0.90, which leads to anomaly correlations less than 0.6. One can notice that the second predictable axis corresponds approximately (part of variance, RMS error, and spatial pattern) to the third EOF. The following predictable axes have no predictive skill.

3.3. *The first persistent axes*

Let us forget in this subsection the ECMWF model and consider the patterns that the smoothed persistence best predicts at 10-day lag. We have carried out the same analysis as in the last subsection, substituting the model forecasts for the observed situations 10 days before; since the RMS error by pure persistence is $(2(1 - AC(10)))^{1/2}$, the axes are arranged in decreasing autocorrelation. If we rearrange the axes in decreasing squared autocorrelation, the first axes maximize the RMS error by smoothed persistence $(1 - AC(10)^2)^{1/2}$. The first persistent axis (Fig. 3) explains 6% of the total variance. The RMS error is $e_1 = 0.81$ but $e_1^* = 0.96$ by the testing procedure, which shows smaller statistical stability in this case. Anyway, since the spatial pattern is approximately the same as the first predictable axis (the negative structure is displaced northwards) we can assume that the order of magnitude of the actual best RMS error by smoothed persistence is about 0.90. It is interesting to notice that the same pattern with minor differences maximizes the variance, the predictability by the model, and the persistence. Moreover the second persistent axis ($e_2 = 0.84$, $e_2^* = 0.94$) the second predictable axis, and the third EOF have similar structures too, mainly

Table 2. *Year-to-year variability of the components corresponding to the first predictable axis: mean observed component m(o), mean predicted component m(p), and correlation coefficient between observed and predicted components c(o,p)*

Winter	1979/80	1980/81	1981/82	1982/83	1983/84	1984/85	1985/86
$m(o)$	0.16	−0.50	0.68	−0.94	0.08	0.81	−0.28
$m(p)$	0.19	−0.39	0.56	−0.57	0.16	0.47	−0.42
$c(o,p)$	0.60	0.54	0.59	0.65	0.35	0.61	0.54

over the Atlantic Ocean where they express a blocking situation (when the component is negative).

3.4. *Discussion*

In the last subsection we have noticed a degeneracy of the first two persistent axes ($e_2^* < e_1^*$) showing the shortness of the 7 winter sample to determine the first persistent axis. In Subsection 3.2, the sample seems to be sufficient to extract the first predictable axis. If we assume that, at the hemispheric scale, two situations separated by a week are independent, the actual sample size is about 100. In order to see whether this size is necessary we have carried out a Predictable Component Analysis with the 1st and the 15th of each month and the 28th February (49 situations). The map of the first axis is quite different from Fig. 2 and the RMS errors are $e_1 = 0.56$, $e_1^* = 1.18$. The previous size is thus necessary and despite the evolution of the ECMWF model we need all the situations available. This is underlined by the high sensitivity of the RMS error to minor changes in the axes (comparison of Fig. 1a with Fig. 2).

In order to measure the impact of the ECMWF improvements on the components corresponding to the first predictable axis, we have calculated for each winter the mean observed component, the mean predicted component, and the correlation coefficient between the observed and predicted component. The results are displayed in Table 2. No systematic trend is found in the averages and we can conclude that the model bias is about the same all during the period (at least along this axis). Moreover, there seems to be a biennial cycle because of the alternating sign of the averages (except in 1984/85). The correlation coefficients do not show a systematic improvement of the model: the best winter is 1982/83 (Fig. 4a), probably because of the "El Niño" event which produced strong Sea Surface Temperature anomalies, the model being able to simulate the atmospheric response to these anomalies; during this winter the mean observed and predicted components reached their maximum absolute value. The worst winter is the following winter (Fig. 4b), anyway the model was able to predict the positive event at the end of January 1984.

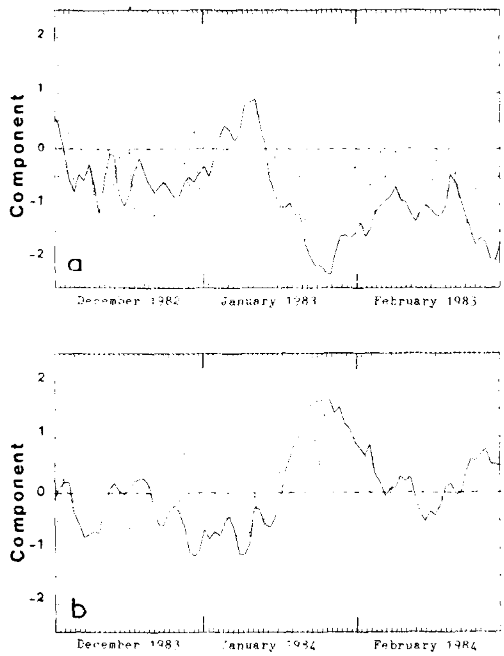

Fig. 4. Time evolution of the components corresponding to the first predictable axis in 1982/83 (a) and 1983/84 (b): observation (solid line) and forecast (dashed line).

We have produced composite maps corresponding to strong positive and strong nega-

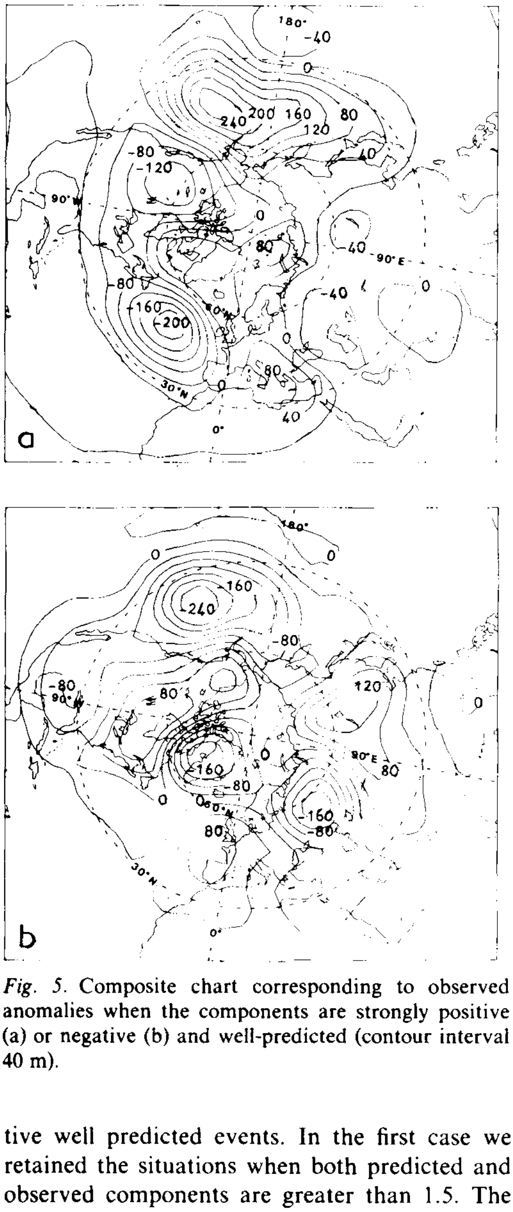

Fig. 5. Composite chart corresponding to observed anomalies when the components are strongly positive (a) or negative (b) and well-predicted (contour interval 40 m).

tive well predicted events. In the first case we retained the situations when both predicted and observed components are greater than 1.5. The dates are:

—31 December 1981;

—1, 2, 10, 11, 13, 14, 15, 17 and 19 January 1982;

—24 January and 20 December 1984;

—6, 7, 8, 9, 10, 18 and 28 February 1985.

The composite map of the observed situations (Fig. 5a) is very similar to the first predictable axis, with a factor of about 2 corresponding to component values between 1.5 and 2.5. The composite map of the corresponding forecasts (not shown) is very similar too; that is not surprising since the forecasts retained have good skill by construction. In the second case we retain the situations when both predicted and observed components are less than -1.5. The dates are:

—13 and 16 January 1981;

—20, 22, 23, 25 January, and 25, 27, 28 February 1983.

The composite map of observed situations (Fig. 5b) presents some differences with the first predictable axis multiplied by -2. This is due to the smaller number of situations than in the positive case, 9 strong negative against 19 strong positive situations; the total number of observed strong negative situations is 37 against 54 strong positive ones although the series is centred. Moreover the resemblance between the observed and the forecast composite maps is less striking than in the positive case; the time mean RMS error of the fields over the whole hemisphere for the strong negative situations (i.e., when both predicted and observed components are less than -1.5) is 89 m against 85 m for the strong positive ones. This does not imply that strong positive anomalies are more predictable by the model than strong negative ones since the composite maps have been built up with the assumption of good predictability. This phenomenon is due to the relative scarcity of the strong negative events. Moreover the strong negative events seem more predictable than the strong positive ones: when the forecast component is less than -1.5 (resp. greater than 1.5) the expected RMS error is 90 m (resp. 101 m). The total mean RMS error being 94 m, we must be *a priori* more confident in a strong negative component than in a strong positive one. Despite the weak percentage of variance explained by the first predictable axis, the pattern may be similar to actual anomalies in some cases.

In a recent study devoted to the predictability of the forecast skill, Palmer and Tibaldi (1986, personal communication) have developed a statistical method which consists of a linear regression of the RMS error by the forecast field. The component they obtain has a time correlation of 0.55 with the first predictable component and the corresponding axis looks like Fig. 2 especially over the Pacific–North America. The geometrical interpretations (in the vector space described by the first 20 EOFs) of the two

Table 3. *RMS error as a function of the lag l (day) for the model forecasts of the first predictable axis at 10-day lag (e_l), of the first EOF (E_l), of the second EOF (E_2), and of the third EOF (E_3); RMS error by smoothed persistence of the first persistent axis at lag l (e^{*}_{pers})*

l	1	2	3	4	5	6	7	8	9	10
e_1	0.17	0.19	0.29	0.37	0.42	0.47	0.50	0.56	0.72	0.76
E_1	0.13	0.17	0.24	0.38	0.47	0.58	0.60	0.64	0.78	1.03
E_2	0.20	0.21	0.26	0.44	0.45	0.52	0.77	0.84	0.90	0.98
E_3	0.27	0.20	0.25	0.31	0.36	0.53	0.75	0.78	0.95	0.91
e^{*}_{pers}	0.26	0.44	0.57	0.66	0.73	0.79	0.84	0.89	0.94	0.96

methods are different: $\underline{A}$ be the first predictable axis and $\underline{B}$ the axis of the regression coefficients (the cosine between $\underline{A}$ and $\underline{B}$ is 0.28). Following the first method, a forecast $\underline{X}$ will be expected better than normal when the angle between $\underline{X}$ and $\underline{A}$ is small (i.e., near to 0 or to π). Following the second method this forecast will be expected better than normal when the projection of $\underline{X}$ on $\underline{B}$ is negative. The first method assumes a symmetry of the anomalies with respect to the skill though the second one assumes that the skill is determined by the sign of the anomaly. The combination of both methods yields a promising way of *a priori* evaluation of the skill. The nonlinear behaviour encountered in the last paragraph may be explained: when the first predictable component is negative, the expected regression component is negative since the two components are correlated and thus the expected RMS error is less than normal.

The last point we shall discuss is whether this first predictable axis has some predictive skill at lower lags; unfortunately, we do not have data at higher lags. If a pattern were predictable only at 10-day lag, it would be a remarkable phenomenon (e.g., 10-day or 20-day oscillation) or most probably an artefact. Table 3 shows the RMS error as a function of the lag for the first predictable axis and the first 3 EOFs, and the RMS error beyond which there is no predictability; this last series is obtained by performing a Persistent Component Analysis at each lag as in Subsection 3.3 and calculating the RMS error e^{*}_1 by the testing procedure previously described. Except for lag 1 (EOF3), lag 9 (EOF3), and lag 10 (EOF1 and EOF2) the EOFs predicted by the ECMWF model have some predictive skill. From lag 1 to 3 the first EOF is the most predictable, from lag 4 to 5 the third EOF overtakes it, and from lags 6 to 10 the first predictable axis has the best skill. For 6- to 9-day lags better skill may be obtained by performing predictable component analyses at each lag but for 9-day lag the improvement is marginal and the pattern similar. The increase of RMS error of the first predictable axis as a function of the lag is quite linear and an extrapolation of Table 3 indicates that this error should attain the predictability limit at 13 day lag. The RMS error e^{*}_1 at 10-day lag being 0.80, we can notice that the model is able to produce at this lag forecasts with a skill that the smoothed persistence cannot reach beyond 6 days.

4. Regional predictability

4.1. The Atlantic–Europe area

The predictability of structures over the whole northern hemisphere is interesting from a theoretical point of view but the smaller scales are more useful for operational forecast. For example the record cold event of January 1985 in France did not appear in the series of components of the first predictable axis. We have thus extracted from the data the midlatitudinal zone between 35°N and 80°N and divided this zone into 3 areas: Atlantic–Europe (85°W–35°E), Asia (40°E–160°E), and Pacific–North America (165°E–80°W). For each area we have performed an EOF analysis, filtered the data by using the first 20 EOFs (the same study as in Subsection 2.2 shows that this number is reasonable), and we have calculated the first predictable axis and the first persistent axis as in Section 3. The first EOF of the Atlantic–Europe area explains 20% of the

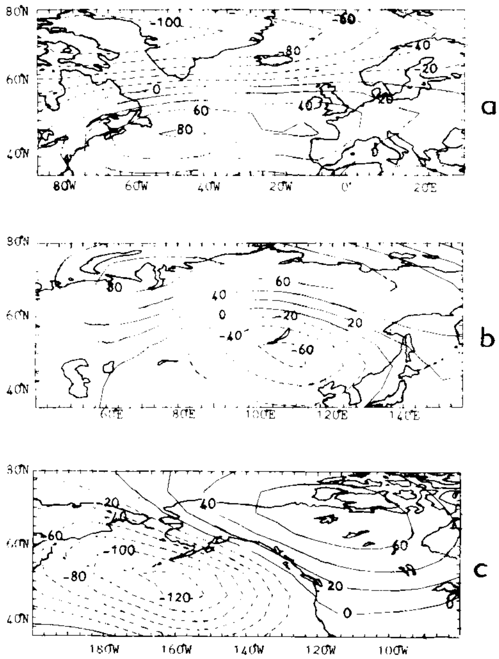

Fig. 6. First predictable axis of the Atlantic–Europe (a), Asia (b), and Pacific America (c) areas (contour interval 20 m; negative contours are dashed).

total variance of this area and exhibits a contrast between latitudes over and under 60° N. The maximum is located over northern Europe and the minimum over Greenland. This phenomenon has been described in the literature as the Greenland Seesaw (van Loon and Rogers, 1978). This EOF has no predictive skill at 10-day lag ($e_1 = 1.0$). The first predictable axis (Fig. 6a) looks like the first EOF except for the location of the maximum over the western Atlantic; it explains 15% of the variance and the predictive skill by the model ($e_1 = 0.86$, $e_1^* = 0.92$) is better than by the smoothed persistence (RMS error of 0.98). The first persistent axis is about the same as the first predictable axis, the maximum over Atlantic being more intense, and its RMS error of 0.94 is hardly superior to the RMS error of the predictable component. So the predictability of the model exists but is marginal.

4.2. The Asian area

This area is not a region of important fluctuation of 500 mb height. The first EOF explains 21% of the variance and corresponds to a seesaw between the north-western and the south-eastern part of the continent. It has no predictive skill ($e_1 = 1.16$). The first predictable axis (Fig. 6b) exhibits the same structure and has no predictive skill ($e_1 = 0.96$, $e_1^* = 1.06$). The only prediction on this area can be made by the first persistent axis which explains 8% of the variance with a RMS error $e_1^* = 0.97$. The spatial pattern differs slightly from Fig. 6b by a lower amplitude of the seesaw and the location of the minimum over Japan instead of China. On this area the ECMWF model has no predictive skill at 10-day lag.

4.3. The Pacific–north America area

This area should have the best predictive skill since the value of the first hemispheric predictable axis is maximum over the Pacific. The first EOF explains 23% of the variance and connects the eastern negatively with the western part of the area, the zero isoline following approximately the 140° W meridian. This phenomenon is described as the Pacific–North America pattern by Wallace and Gutzler (1981). This EOF has no predictive skill ($e_1 = 1.06$). The first predictable axis (Fig. 6c) presents a slight modification to this pattern: the maximum (over the continent) is displaced northwards and the minimum (over the ocean) southwards. It explains 17% of the variance and its predictive skill is a little bit lower than the first hemispheric predictable axis ($e_1 = 0.80$, $e_1^* = 0.83$) but is not negligible. The first persistent axis is quite the same as the first predictable axis and the RMS error by smoothed persistence is slightly improved (0.91 instead of 0.92).

5. Concluding remarks

The conclusion of this study is that there exists in the northern hemisphere winter 500 mb height a structure that explains 8% of the variance of the field and which is predicted at 10-day lag by the ECMWF model with an RMS error of 0.8 standard deviations (i.e. correlation coefficient 0.7). On smaller scales the predictability vanishes except over Pacific–North America and in any case the best predicted structures are the restriction of the hemispheric pattern to the area. This hemispheric structure looks like the mode of maximum variability with a geographical distribution widely imposed by the large scale orography (zonal wavenumber 2). This structure is also, with some minor differences, the pattern that the smoothed persistence best predicts, but with a lower skill. The mechanism responsible for this predictability is probably the good dealing of the large scale waves by the model up to 4–6 day lag associated with their persistence. The application of these results to operational 10-day forecasting is not great: one can set more confidence on a 10-day anomaly forecast that looks like Fig. 2; more generally one can attempt to predict the forecast skill by looking at the relative part of the components corresponding to the first predictable axes for a given forecast. The method can be improved by taking into account a linear regression of the RMS by the forecast, that involves the sign of the anomaly. Anyway these results underline the fact that it is useful to run the ECMWF model up to 10 days since 10 day anomaly forecasts are significantly different from noise. Moreover, because of the constant improvement of the model, there exist perhaps structures (that we are now unable to exhibit due to the shortness of the sample size when restricted to winter 1985/86) which the most recent version can predict with greater skill.

The method described in this paper is more promising in Dynamical Extended Range Forecasting (DERF) when long enough samples become available. In this case the number of forecasts necessary to ensure statistical stability will probably be less than the number necessary in the present study. Namely we can assume that a structure well predicted at 20-day lag must also be well predicted at 25-day lag and the sample will contain forecasts at different lags; if Monte Carlo or Lagged Average forecasts are performed the sample size will also increase. Another solution in DERF is to consider time averaged situations which have smoother spatial structures than individual situations and can be reasonably described by 5 EOFs instead of 20: the number of degrees of freedom being smaller, the sample size may be reduced. Perhaps in this latter case the first EOFs will provide a sufficient filter to separate the part of the field that a model can predict from the remaining widely dominated by the model noise.

6. Acknowledgements

I express my thanks to J. C. Andre and M. Jarraud for their stimulating discussions, and to S. Tibaldi for his helpful comments. I would like to acknowledge ECMWF which provides analyses and forecasts to the member states in a very convenient format. This work was partly supported by PNEDC (National Program for Studies of Climate Dynamics).

7. Appendix. Predictable component analysis

Let us consider the expansions of an observed field $X(\mathbf{x}, t)$ and its corresponding prediction $X^{\mathrm{P}}(\mathbf{x}, t)$ (after having removed the time averages $\overline{X(\mathbf{x})}$ and $\overline{X^{\mathrm{P}}(\mathbf{x})}$) in the first n EOFs of the observed dataset:

$$X(\mathbf{x}, t) = a_1(t)\, A_1(\mathbf{x}) + \ldots + a_n(t)\, A_n(\mathbf{x}) + R_n(\mathbf{x}, t), \tag{A1a}$$

$$X^{\mathrm{P}}(\mathbf{x}, t) = a_1^{\mathrm{P}}(t)\, A_1(\mathbf{x}) + \ldots + a_n^{\mathrm{P}}(t)\, A_n(\mathbf{x}) + R_n^{\mathrm{P}}(\mathbf{x}, t), \tag{A1b}$$

with:

$$(1/T) \sum_{t=1}^{T} a_i(t) = (1/T) \times \sum_{t=1}^{T} a_i^{\mathrm{P}}(t) = 0 \quad \text{for } i = 1, \ldots, n, \tag{A2}$$

$$(1/T) \sum_{t=1}^{T} a_i(t)\, a_j(t) = 1 \quad \text{if } i = j, \quad = 0 \text{ otherwise.} \tag{A3}$$

We introduce a rotation matrix M satisfying:

$$\sum_{k=1}^{n} M_{ik}\, M_{jk} = \sum_{k=1}^{n} M_{ki}\, M_{kj} = 1 \quad \text{if } i = j, \quad = 0 \text{ otherwise.} \tag{A4}$$

The rotated axes $B_i(\mathbf{x})$ are defined by:

$$B_i(\mathbf{x}) = \sum_{j=1}^{n} M_{ij}\, A_j(\mathbf{x}). \tag{A5}$$

and the rotated components $b_i(t)$ and $b_i^{\mathrm{P}}(t)$ by:

$$b_i(t) = \sum_{j=1}^{n} M_{ij}\, a_j(t), \tag{A6a}$$

$$b_i^{\mathrm{P}}(t) = \sum_{j=1}^{n} M_{ji}\, a_j^{\mathrm{P}}(t), \tag{A6b}$$

The b_i's and b_i^{P}'s satisfy Condition (A2), the b_i's satisfy Condition (A3), and X and X^{P} may be expanded following (4a) and (4b). We choose M in order to get minimum values for e_i^2:

$$e_i^2 = (1/T) \sum_{t=1}^{T} (b_i(t) - b_i^{\mathrm{P}}(t))^2 \tag{A7}$$

M_{ij} is the ith coordinate of the jth eigenvector (arranged in increasing eigenvalues) of the symmetrical positive matrix E:

$$E_{ij} = (1/T) \sum_{t=1}^{T} (a_i(t) - a_i^{\mathrm{P}}(t))(a_j(t) - a_j^{\mathrm{P}}(t)). \tag{A8}$$

The eigenvalues of E are the e_i^2's, since one can write:

$$e_i^2 = \sum_{k=1}^{n} \sum_{j=1}^{n} M_{ki}\, E_{kj}\, M_{ji}. \tag{A9}$$

The persistent axes (C_i) and components (c_i and c_i^{P}) at lag 1 are obtained in the same way by replacing $a_i^{\mathrm{P}}(t)$ by $a_i(t-1)$.

REFERENCES

Cubasch, U. and Wiin-Nielsen, A. C. 1986. Predictability studies with the ECMWF spectral model for the extended range: the impact of horizontal resolution and sea surface temperature. *Tellus 38A*, 25–41.

Déqué, M. 1986a. On the comparison between two sets of 500 mb height eigenfunctions. *Tellus 38A*, 448–452.

Déqué, M. 1986b. Maximization of the predictability of a meteorological field (in French). *Rev. Stat. Appl. 35*, 17–25.

Hoffman, N. R. and Kalnay, E. 1983. Lagged average forecasting, an alternative to Monte Carlo forecasting. *Tellus 35A*, 100–118.

Holmström, I. 1963. On a method for parametric representation of the state of the atmosphere. *Tellus 15*, 127–149.

Lorenz, E. N. 1956. Empirical orthogonal functions and statistical weather prediction. *Scientific report no 1*, Dept. of Meteorology, Massachusetts Institute of Technology, Cambridge, Massachusetts, USA.

Miyakoda, K., Sirutis, J. and Ploshav, J. 1986. Monthly forecast experiments. Part I: without anomaly forcings. *Long-Range Forecasting Research Report Series No 6 (WMO)*, 550–554.

Peagle, N. J. and Haslam, R. B. 1982. Empirical orthogonal function estimates of local predictability. *J. Appl. Meteorol. 21*, 117–126.

van Loon, H. and Rogers, J. C. 1978. The seesaw in winter temperature between Greenland and northern Europe. *Mon. Wea. Rev. 106*, 296–316.

Volmer, J. P., Déqué, M. and Rousselet, D. 1984. The EOF analysis of 500 mb height: a comparison between simulation and reality. *Tellus 36A*, 336–347.

Wallace, J. M. and Gutzler, D. S. 1981. Teleconnections in the geopotential height field during the northern hemisphere winter. *Mon. Wea. Rev. 109*, 784–812.